Boletim da Sociedade Astronômica Brasileira, **32**, no. 1, 25-29
© SAB 2020

The 6–9 μm polycyclic aromatic hydrocarbon bands in starburst-dominated sources

C. Canelo[1], A. Friaça[1], D. Sales[2], & M. Pastoriza[3]

[1] Departamento de Astronomia, Instituto de Astronomia, Geofísica e Ciências Atmosféricas, Universidade de São Paulo, 05508-090 São Paulo, Brazil e-mail: camcanelo@gmail.com, amancio.friaca@iag.usp.br
[2] Instituto de Matemática, Estatística e Física, Universidade Federal do Rio Grande, Rio Grande 96203-900, Brazil e-mail: dinalvaires@gmail.com
[3] Departamento de Astronomia, Instituto de Física, Universidade Federal do Rio Grande do Sul, Rio Grande do Sul, Brazil e-mail: miriani.pastoriza@ufrgs.br

Abstract. The main reservoir of molecular organic material in space is in the form of polycyclic aromatic hydrocarbons (PAHs). They are of a great astrochemical and astrobiological interest due to their potential to form prebiotic molecules. For instance, their simplest units with N atoms included in the aromatic rings, denominated Polycyclic Aromatic Nitrogen Heterocycles (PANHs), are involved in the production of Nucleobases. Analyses of the PAH features profiles, especially the 6.2, 7.7 and 8.6 μm mid-infrared (MIR) bands, could indicate their presence in astrophysical environments of galaxies. In this work, 126 predominantly starburst-dominated galaxies (including HII regions and Seyferts, for example), extracted from the Spitzer/IRS ATLAS project, have these bands fitted allowing their separation into the Peeters' A, B and C classes. The blueshift of the 6.2 μm PAH emission band, typical for a class A object, was attributed to PANH molecules and seems to dominate this spectral feature in starburst-dominated galaxies, suggesting a significant presence of these molecules. The 7.7 μm complex is also dominated by class A objects in this sample while 8.6 μm band presented more class B sources. The higher correlation between 6.2 and 7.7 μm bands is expected due to their same CC vibration mode. Considering just the class A objects for the 6.2 μm band, 63% of them received the same classification for the 7.7 μm band. Although this result does not allow us to indirectly study the PANHs emission at 6.2 μm with the other bands correlation, it supports the complexity of PAH emission. The differences in the profiles, even for the same source, arise from the astrophysical and chemical conditions of the environments, including all the molecular species that contribute differently for each band emission.

Resumo. O principal reservatório de material molecular orgânico no espaço está na forma de hidrocarbonetos policíclicos aromáticos (PAHs). Eles são de grande interesse astroquímico e astrobiológico devido ao seu potencial para formar moléculas prebióticas. Por exemplo, suas unidades mais simples com átomos de N incluídos nos anéis aromáticos, denominados heterociclos policíclicos aromáticos nitrogenados (PANHs), estão envolvidos na produção de nucleobases. Análises dos perfis de PAH, especialmente as bandas de 6.2, 7.7 e 8.6 μm do infravermelho médio (MIR), podem indicar sua presença em ambientes astrofísicos de galáxias. Neste trabalho, 126 galáxias predominantemente dominadas por emissão de *starbursts* (incluindo regiões HII e Seyferts, por exemplo), extraídas do projeto Spitzer/IRS ATLAS, tiveram essas bandas ajustadas, permitindo a separação nas classes A, B e C de Peeters. O desvio para o azul da banda de emissão de PAH de 6.2 μm, típico de um objeto da classe A, foi atribuído às moléculas de PANH e parece dominar essa característica espectral nas galáxias dominadas por *starbursts*, sugerindo uma presença significativa dessas moléculas. O complexo de 7.7 μm também é dominado por objetos de classe A nesta amostra, enquanto a banda de 8.6 μm apresentou mais fontes de classe B. A correlação mais alta entre as bandas de 6.2 e 7.7 μm é esperada devido ao mesmo modo de vibração CC. Considerando apenas os objetos da classe A para a banda de 6.2 μm, 63% deles receberam a mesma classificação para a banda de 7.7 μm. Embora esse resultado não nos permita estudar indiretamente a emissão de PANHs em 6.2 μm com a correlação de outras bandas, ele suporta a complexidade da emissão de PAH. As diferenças nos perfis, mesmo para a mesma fonte, surgem das condições astrofísicas e químicas dos ambientes, incluindo todas as espécies moleculares que contribuem diferentemente para cada banda de emissão.

Keywords. galaxies: starburst – infrared: ISM – Astrobiology

1. Introduction

PAHs (Polycyclic Aromatic Hydrocarbons) represent the dominant organic material in space (Ehrenfreund et al. 2006). Their simplest units with N atoms included in the aromatic rings, denominated Polycyclic Aromatic Nitrogen Heterocycles (PANHs), are involved in the production of Nucleobases. They are also present in meteorites (e.g. Murchison, Callahan et al. 2008) and must have been transported almost intact to terrestrial planets such as Earth and Mars. These facts give support to the idea of their contribution to the origins of life on Earth and elsewhere, since they could also form nucleobase-type structures in the ISM (Elsila et al. 2006; Parker et al. 2015).

Analyses of the PAH features profiles, especially the 6.2, 7.7 and 8.6 μm mid-infrared (MIR) bands, could indicate their presence in astrophysical environments of galaxies. The observed blueshift of the 6.2 μm band in several astrophysical sources has only been well reproduced by emission of PANH molecules (Hudgins et al. 2005) and was attributed to these molecules. Such spectral signature is commonly observed towards starburst-dominated galaxies, suggesting a significant presence of PANHs in these sources (Canelo et al. 2018).

The correlation between the PAH bands due to their vibration modes, specially the 6.2 and 7.7 μm bands, could furnish another strategy for deriving the variations of the 6.2 μm profile. Both features are produced by the CC vibration mode. The 8.6 μm band could also be connected to the other bands in spite of being produced by the CH vibration mode. It is also possible to distribute these bands into the Peeters' A, B and C classes (Peeters et al. 2002) depending on their central wavelength. The

Table 1. Profile peak positions for each Peeters' classes. $F_{7.6}/F_{7.8}$ represents the flux ratio between 7.6 and 7.8 μm features.

Class	6.2 μm	7.7 μm	8.6 μm
A	< 6.23	~ 7.6	< 8.6
		($\frac{F_{7.6}}{F_{7.8}} > 1.1$)	
AB	——	($\frac{F_{7.6}}{F_{7.8}} = 1\pm0.1$)	——
B	6.23<λ<6.29	~ 7.8	> 8.6
		($\frac{F_{7.6}}{F_{7.8}} < 0.9$)	
C	> 6.29	~ 8.22	——

bands can be connected to each other in some cases, mainly for class A objects (van Diedenhoven et al. 2004).

2. Data analysis

In this work, we studied 126 starburst-dominated galaxies extracted from the Spitzer/IRS ATLAS project (Hernán-Caballero & Hatziminaoglou 2011). Despite the starburst-dominated emission of our objects, they can be also from different types such as ULIRG (Ultra Luminous Infrared Galaxy), Seyfert and LINER (Low-Ionisation Nuclear Emission-line Region). These galaxies have their 6.2, 7.7 and 8.6 μm PAH profiles fitted allowing the distribution of the sources into the Peeters' A, B and C classes according to Tab. 1. The classes depend basically on the peak position of the bands. However, the 7.7 μm complex present two features at 7.6 and 7.8 μm. In order to classify this complex, we used the flux ratio of both features to distinguish which one was dominating the emission, as shown in Tab. 1.

Before the fitting of the PAH profiles, the continuum was decomposed with a local spline and subtracted from the spectra (for more details, see Peeters et al. 2017; Canelo et al. 2018). This spline considers an anchor point near 8.2 μm which allows the independent fitting of the 7.7 μm complex and the 8.6 μm feature (Brandl et al. 2006). The local spline decomposition for two galaxies is displayed in Fig. 1. The 6.2 μm band has already been studied with a Gaussian fit through the PYTHON submodule *scipy.curve_fit* (Canelo et al. 2018). Following the same procedure, three Gaussian profiles were used to estimate the 7.6, 7.8 and 8.6 μm features. The amplitude, central wavelength and full width at half maximum (FWHM) were considered as free parameters during the fitting for all bands. In order to compare the PAH features, we also calculated the flux intensities by integration of the fitted Gaussian profiles in the intervals of 6.1 – 6.35 μm for the 6.2 μm band; 7.2 – 8.2 μm for the 7.6 and 7.8 μm components; and 8.2 – 9 μm for the 8.6 μm band.

3. Results

Concerning the 6.2 μm PAH band, some galaxies present a red tail, as shown in Fig. 2. This tail could be just an expected feature of the asymmetry of the profile (Tielens 2008) and was excluded from the fitting. Nevertheless, it could also be a fainter emission of PAH cations (Hudgins et al. 2005), PAHs with aliphatic features (Pino et al. 2008) or perylene-like structures (Candian et al. 2014), and C_{60}^{+} (Berné et al. 2015). Moreover, this band can be fitted with two Gaussian components to account for this second feature (for more details, see Canelo et al. 2018).

The Gaussian fit of the 7–9 μm region is exemplified in Fig 3 . In general, the 7.7 μm features present higher intensities than the 8.6 μm feature. However, the relative intensities between them vary according to the object. In order to better comprehend the variations between the bands, Figure 4 compares the

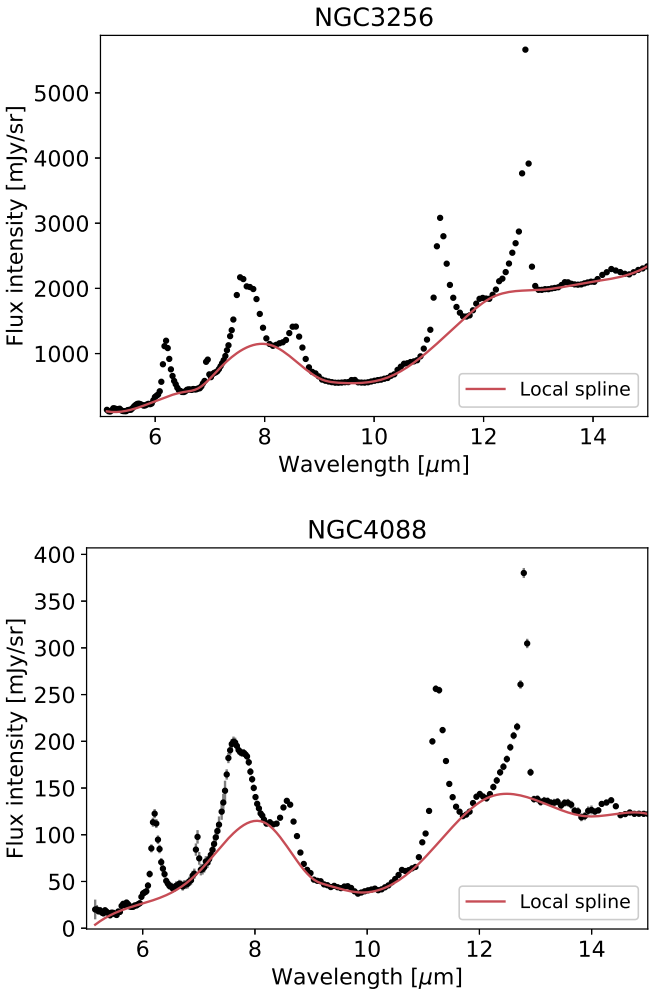

Figure 1. Local spline decomposition of the continuum emission represented by the red line for NGC3256 and NGC4088.

flux ratios of $F_{7.6}/F_{6.2}$ and $F_{8.6}/F_{6.2}$, which do not seem to be influenced by the different types of objects. These ratios must be connect to physical conditions and the dominant PAH population of the galaxies. The relative intensity of the 7.7 and 6.2 μm bands

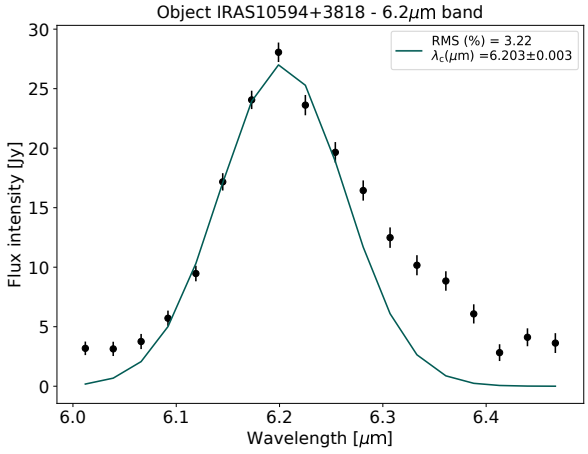

Figure 2. Gaussian fit of the 6.2 μm band for object IRAS10594+3818 (Canelo et al. 2018).

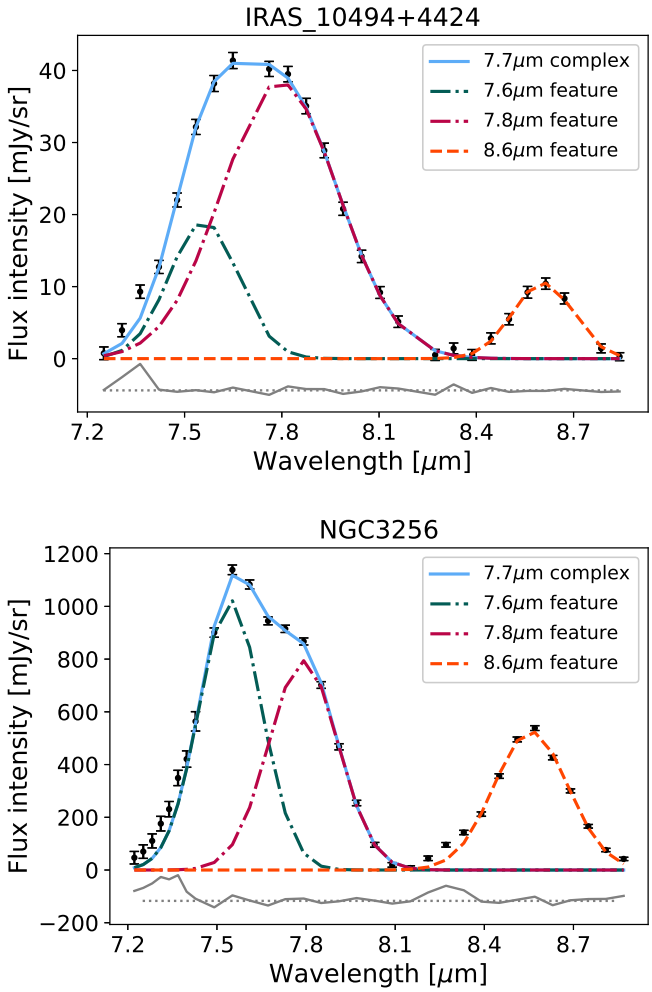

Figure 3. Gaussian fit results – the solid blue line represents the total fit for the 7.7 μm complex with two Gaussian components respectively identified in the label. The individual Gaussian of the 8.6 μm band is also shown (Canelo et al. *in prep.*).

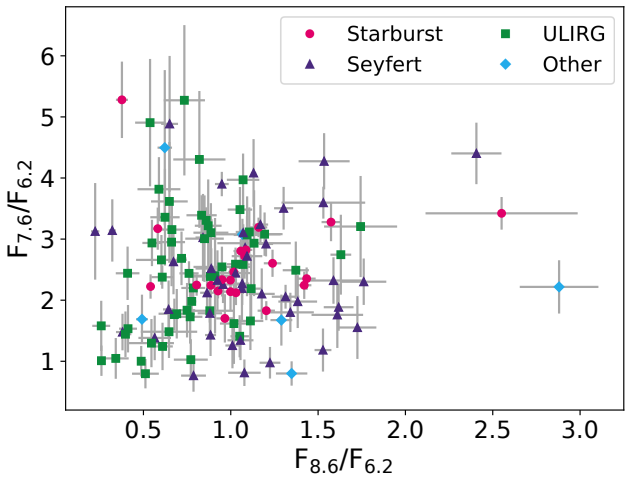

Figure 4. Comparison of the flux intensities of the 7.6 and 8.6μm bands obtained for each galaxy normalized for the 6.2μm band. Their types were divided into four main groups with data points represented by the symbols labeled in the legend. The uncertainties are displayed as gray error bars (Canelo et al. *in prep.*).

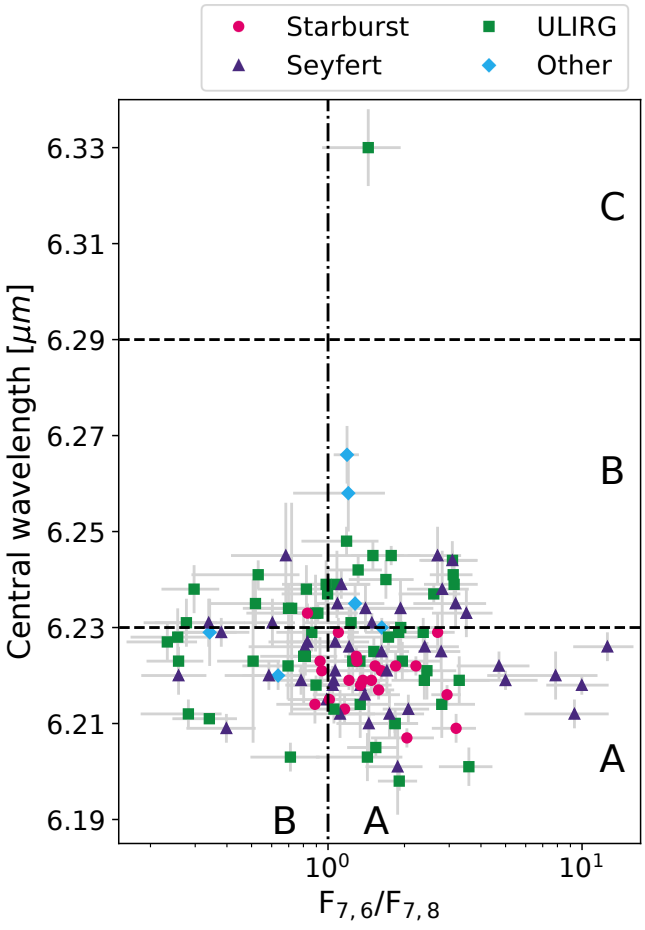

Figure 5. Relation between the flux ratio $F_{7.6}/F_{7.8}$ through the peak position of the 6.2 μm band. The type of the galaxies were also divided into four main groups. Horizontal dashed lines represents the limits of the Peeters' classes which are also indicated by the letters (Canelo et al. *in prep.*).

is greater than 1 for PAHs with even number of carbons and less than 1 for odd-carbon PAHs (Ricca et al. 2018). However, their relative intensities are not expected to track PAH size effectively due to the mixed distribution of sizes throughout this range (Maragkoudakis et al. 2018).

An overview of the Peeters' classification for our sample can be seen in Tab. 2. Class A objects dominate the 6.2 and 7.7 μm profiles while the 8.6 μm band is mainly represented by class B objects. Considering class A objects, 68% galaxies received the "A" classification for the 6.2 μm band and 43% received "A A" for the 6.2 and 7.7 μm bands. This corroborates the strong correlation between both bands. On the other hand, only 18% galaxies received the "A A A" classification for the three bands. This could indicate a minor correlation with the 8.6 μm band, which can be expected due to the different vibration mode (CH) that is responsible for this band. The 6.2 μm band is the only one to present a class C profile and there are also few class AB profiles for the 7.7 μm complex.

The class A domination in the 6.2 and 7.7 μm bands is expected because class A objects are the most common in the Universe and embrace several astrophysical sources (Pino et al. 2008). As can be reinforced by Fig. 5, class A objects are more correlated than the others – most of the sources

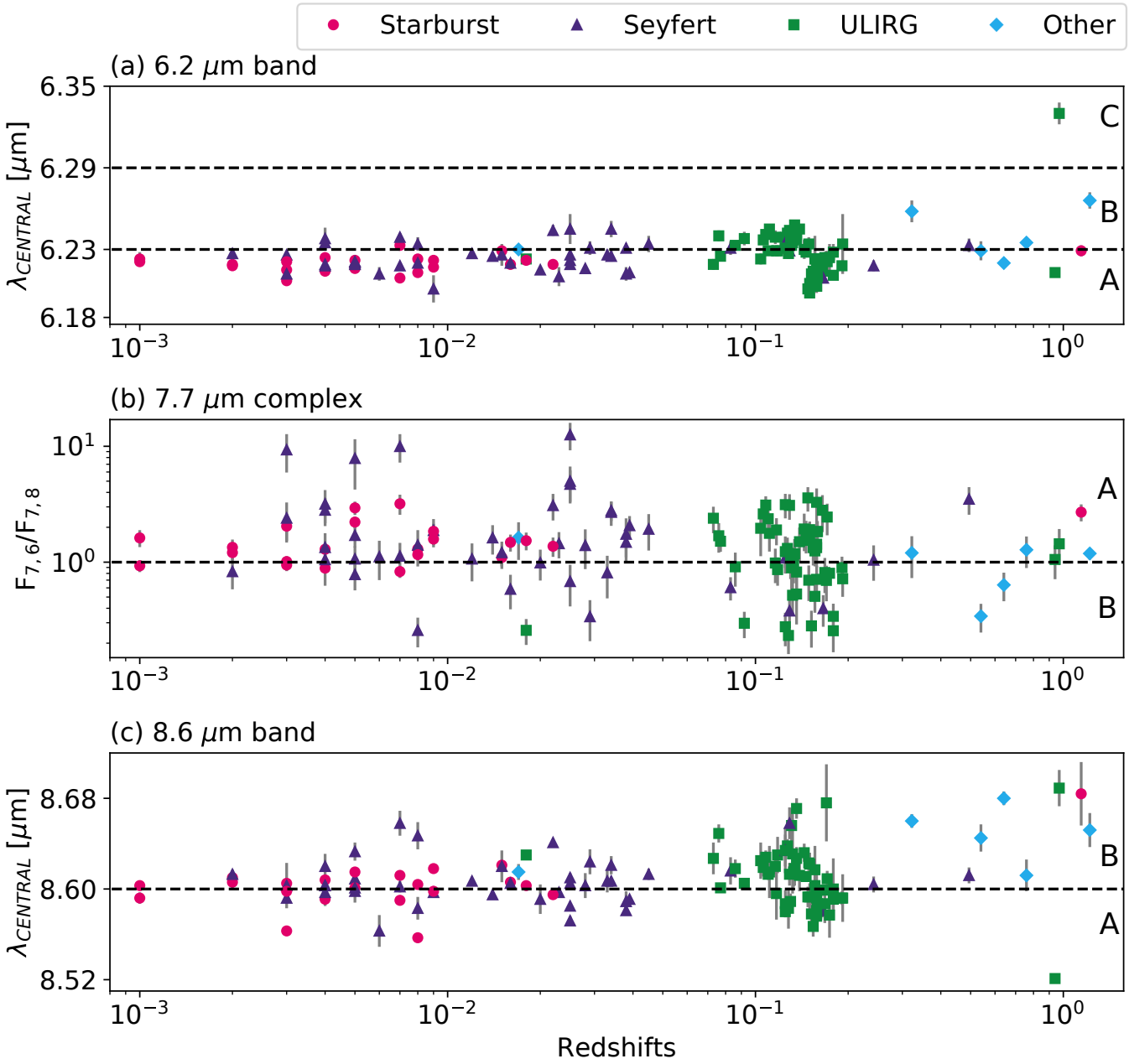

Figure 6. Distribution of the 6.2, 7.7 and 8.6 μm bands, respectively, according to the galaxies redshift. The dashed lines are the limits among the Peeters' classes, indicated also by A, B or C letter. The redshift axis is in logarithmic scale. The type of the galaxies were also divided into four main groups. The uncertainties are displayed as gray error bars. (Canelo et al. *in prep.*).

Table 2. Profile distribution of the 126 studied galaxies into the Peeters' class.

Band (μm)	**Class A** (%)	**Class B** (%)	**Class AB** (%)	**Class C** (%)
6.2	68	31	—	1
7.7	61	27	12	—
8.6	37	63	—	—

received the "A" classification for both bands. From the 6.2 μm class A objects, 63% obtained the same classification for the 7.7 μm complex. It is also interesting to notice that starbursts are the mainly class A objects while the other types are more sparsely distributed in the plot. Although the 7.7 μm complex is not necessarily connect to a possible PANH emission such as the 6.2 μm band, galaxies equally classified as A objects for both bands could fortify the veracity of the results.

In Fig. 6 is shown the distribution of the classes along with the redshift of the galaxies. It is possible to perceive the predominance of class A objects over class B objects for the 6.2 and the 7.7 μm bands. The opposite occurs for the 8.6 μm band. The type of the galaxies does not seem to interfere with the classification. Instead, the redshift may play an important role in the results. For all three bands, the quantity of class B sources seems to increase with higher redshifts, which may suggest a evolutionary timescale of the PAH population. We can also realize that lower $F_{7.6}/F_{7.8}$ ratios only occurs for redshifts higher than 0.008 indicating a greater predominance of the 7.8 μm component to the 7.7 μm complex. This feature has

also been attributed to evaporating very small grains (eVSGs, Rapacioli et al. 2005; Berné et al. 2007).

4. Conclusion

We have analyzed the 6.2, 7.7 and 8.6 μm PAH bands of 126 starburst-dominated galaxies, searching for the contribution of the Peeters' classes to the total sample. The predominance of class A objects for the 6.2 μm band could suggest the ubiquity of PANHs to this emission (Canelo et al. 2018). This class is also dominant for the 7.7 μm complex, supporting the strong correlation of these bands as expected due to the same CC vibration mode. Moreover, from the galaxies classified as "A" for the 6.2 μm band, 63% received the same "A" classification for the 7.7 μm complex. This fact could fortify the veracity of our results, although it may not allow us to use the bands correlation to indirectly study the PANHs emission at 6.2 μm. On the other hand, the 8.6 μm band is dominated by class B sources.

The different types of galaxies do not seem to interfere in the results. The variations in the profiles must be connected to the different physical and chemical conditions of the astrophysical environments. Nevertheless, an evolutionary timescale of PAHs can be perceived in Fig. 6. Higher redshift galaxies are more commonly classified as B objects while class A sources are more frequent at lower redshifts. In this sense, it would be important to study higher redshift sources in order to better comprehend this possible PAH evolutionary timescale. The James Webb Space Telescope (JWST) could furnish high resolution data to approach this issue.

Acknowledgements. CMC acknowledges the support of CNPq, Conselho Nacional de Desenvolvimento Científico e Tecnológico - Brazil, process number 141714/2016-6. This study was financed in part by the Coordenação de Aperfeiçoamento de Pessoal de Nível Superior - Brasil (CAPES) - Finance Code 001. DAS acknowledges the support of CNPq and FAPERGS.

References

Berné O., Montillaud J., Joblin C., 2015, A&A, 577, A133
Berné et al., 2007, A&A, 469, 575.
Brandl et al., 2006, ApJ, 653, 1129.
Callahan et al., 2008, Spectrochimica Acta Part A, 71, 1492.
Candian A., Sarre P. J., Tielens A. G. G. M., 2014, ApJ, 791, L10
Canelo et al., 2018, MNRAS, 475, 3746.
Canelo et al., in preparation
Ehrenfreund et al., 2006, Astrobiology, 6, 490.
Elsila et al., 2006, Meteoritics and Planetary Science, 41, 785
Hernán-Caballero & Hatziminaoglou 2011, MNRAS, 414, 500.
Hudgins et al. 2005, ApJ, 632, 316.
Maragkoudakis et al. 2018, MNRAS, 481, 5370
Parker et al. 2015, ApJ, 803, 53.
Peeters et al. 2002, 390, 1089.
Peeters et al. 2017, ApJ, 836, 198.
Pino, et al., 2008, A&A, 490, 665.
Rapacioli M., Joblin C., Boissel P., 2005, A&A, 429, 193.
Ricca et al. 2018, ApJ, 854, 11
Tielens A. G. G. M., 2008, ARA&A, 46, 289
van Diedenhoven et al. 2004, ApJ, 611, 928.